

---

# Weakly-Supervised Camouflaged Object Detection with Scribble Annotations

---

**Ruozhen He\***

Department of Computer Science  
City University of Hong Kong  
ruozhenhe-c@my.cityu.edu.hk

**Qihua Dong\***

Department of Computer Science  
City University of Hong Kong  
dongqh078@gmail.com

**Jiaying Lin**

Department of Computer Science  
City University of Hong Kong  
jiayinglin5-c@my.cityu.edu.hk

**Rynson W.H. Lau**

Department of Computer Science  
City University of Hong Kong  
rynson.lau@cityu.edu.hk

## Abstract

Existing camouflaged object detection (COD) methods rely heavily on large-scale datasets with pixel-wise annotations. However, due to the ambiguous boundary, it is very time-consuming and labor-intensive to annotate camouflage objects pixel-wisely (which takes ~60 minutes per image). In this paper, we propose the first weakly-supervised camouflaged object detection (COD) method, using scribble annotations as supervision. To achieve this, we first construct a scribble-based camouflaged object dataset with 4,040 images and corresponding scribble annotations. It is worth noting that annotating the scribbles used in our dataset takes only ~10 seconds per image, which is 360 times faster than per-pixel annotations. However, the network directly using scribble annotations for supervision will fail to localize the boundary of camouflaged objects and tend to have inconsistent predictions since scribble annotations only describe the primary structure of objects without details. To tackle this problem, we propose a novel consistency loss composed of two parts: a reliable cross-view loss to attain reliable consistency over different images, and a soft inside-view loss to maintain consistency inside a single prediction map. Besides, we observe that humans use semantic information to segment regions near boundaries of camouflaged objects. Therefore, we design a feature-guided loss, which includes visual features directly extracted from images and semantically significant features captured by models. Moreover, we propose a novel network that detects camouflaged objects by scribble learning on structural information and semantic relations. Our network has two novel modules: the *local-context contrasted (LCC) module*, which mimics visual inhibition to enhance image contrast and sharpness in order to expand the scribbles into potential camouflaged regions, and the *logical semantic relation (LSR) module*, which analyzes the semantic relation of the scene to determine the regions representing the camouflaged object. Experimental results show that our model outperforms relevant state-of-the-art methods on three COD benchmarks with an average improvement of 11.0% on MAE, 3.2% on S-measure, 2.5% on E-measure and 4.4% on weighted F-measure.

---

\*Equal contributions.

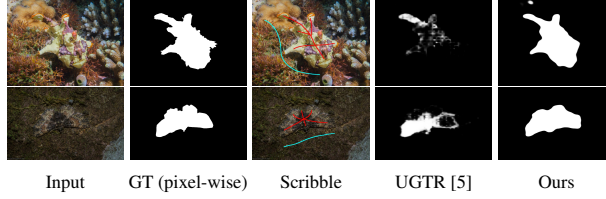


Figure 1: Pixel-wise annotation’s assigning equal significance to each pixel may mislead the model to learn wrong primary structures. Scribble annotates the primary structure of objects (cyan for background, red for foreground). Our method exploits this property to learn rich semantic and structural information from the sparse labels. In some cases, it performs even better than SOTA models under fully supervision.

## 1 Introduction

Camouflaged object detection (COD) aims to detect visually inconspicuous objects in their surroundings. Camouflaged objects include natural objects with protective coloring, small sizes, occlusion, and artificial objects with information hiding purposes. Ambiguous boundaries between objects and backgrounds make it a more challenging task than other object detection tasks. COD have other applications, including medical image segmentation [1, 2], and search and rescue [3].

Although COD methods have been widely studied and achieved excellent performances recently, they rely heavily on large-scale datasets with pixel-wise annotations. There are two main weaknesses for pixel-wise annotation. First, pixel-wise annotation is time-consuming. It takes  $\sim 60$  minutes to annotate one image [4]. Second, pixel-wise annotation assigns equal significance to each object pixel, which may cause the model to fail to learn primary structures. On the contrary, scribble annotations, using lines to label the foreground and background partially, only cost around 10 seconds which is 360 times faster than pixel-wise annotations. See details in Figure 1. Due to the lack of COD datasets with scribble annotations, we propose the first scribble-based COD dataset, named S-COD, which includes 4,040 images from the existing COD datasets [4, 3] and corresponding scribble annotations. Our dataset covers large types of camouflaged objects with primary structure scribble annotations.

However, how to exploit scribbles annotation for camouflaged object detection is still under exploration. Although there exists scribble-based SOD methods SS [6] and SCWS-SOD [7], directly applying them is not appropriate for camouflaged object detection, since camouflaged objects are not salient. Figure 2 shows that existing state-of-the-art scribble-based SOD methods fail in two common but challenging scenarios. The first row of Figure 2 shows a scenario with ambiguous boundaries and a generally consistent background. Due to the consistent low-level features inside objects, SS and SCWS-SOD experience difficulties recognizing the boundary and producing prediction maps with low confidence. The second row requires detectors to identify high-level semantic relations, as more than one object looks like the "camouflaged" foreground. In these scenarios, semantic information is needed to distinguish the real foreground and

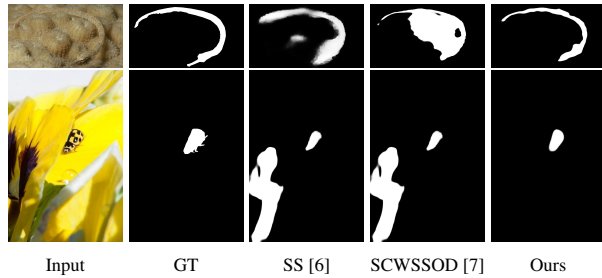


Figure 2: Two popular scenarios where existing scribble-supervised SOD methods SS[6] and SCWSSOD [7] fail. The first row provides simple logic semantic relation, consistency in foreground and background, and ambiguous boundaries which require excellent ability of detecting low-level information (*e.g.*, texture, color) differences. The second row provides obvious low-level contrasts, and complex logical semantic information inside backgrounds (*e.g.*, flower stems and petals), which needs to further identified by logical semantic relation information. Therefore, our method can learn challenging low-level contrasts and logical semantic relations from scribbles.

background parts (*e.g.*, flower stems and petals). Here, both SS and SCWSSOD mistakenly include the wrong objects in the foreground due to poor semantic information learning.

In this paper, we aim to address the weakly-supervised camouflaged object detection problem with scribble annotations. We propose the first scribble-based COD learning framework, consisting of novel loss functions and a network. We observe that humans distinguish the possible foreground objects at first [8], then use semantic information to verify [9], and finally focus on significant features (exclude features that are similar between "camouflage" foreground and background) to clearly segment the boundary of camouflaged objects. To incorporate this process in our models, we propose a feature-guided loss considering not only visual affinity but also higher level features to guide the predictions in boundary regions (like semantics, textures, and shape). Besides, we notice that current weakly supervised methods tend to have inconsistent predictions in COD, possibly due to confusion caused by the "camouflage" characteristic of the foreground. Therefore, we design a stronger and more reliable consistency regularization than previous weakly-supervised learning methods. To be specific, we induce the reliability bias, which has been ignored, to improve self-supervised-fashion consistency constraints and propose the inside-view consistency. These make our model produce reliable predictions with high confidence for camouflaged objects. Moreover, in the design of the network, we propose the local-context contrasted (LCC) module mimicing visual inhibition to strength contrast [10] to find potential camouflaged regions around scribbles, and the logical semantic relation (LSR) module to determine final camouflaged object regions.

In conclusion, our main contributions are generally summarized as follows:

- We propose the first weakly supervised COD dataset with scribble annotation. It accelerates the annotation time to  $\sim 10$  seconds per image, which is 360 times faster than the pixel-wise's. Additionally, it overcomes pixel-wise annotation's limitation of equal significance assignment to every object pixel. Our method tends to have better command of object's main body by scribble learning.
- We propose the first end-to-end weakly supervised training framework for COD. It consists of novel consistency loss functions to impose stronger and more reliable consistency constraints to models, and feature-guided loss functions utilizing high-level semantically significant features targeted at COD tasks.
- We propose a novel network for scribble learning, depending on observations that camouflaged objects generally have low-level contrasts (*e.g.*, texture, color, and intensity) or logical semantic discontinuity (*e.g.*, different objects) with the background. Low-level contrasts expand scribbles to wider likely camouflaged regions, and logical semantic information finalizes the objects.
- Experimental results show that our model outperforms relevant state-of-the-art methods on three COD benchmarks with an average improvement of 11.0% on MAE, 3.2% on S-measure, 2.5% on E-measure and 4.4% on weighted F-measure.

## 2 Related Work

**Scribble-based Weakly Supervised Learning.** Scribble-based learning has been widely used in computer vision tasks such as semantic segmentation [11, 12] and salient object detection [6, 7]. Zhang *et al.* [6] adopt a multi-stage framework with an auxiliary edge detection task for scribble learning. Yu *et al.* [7] propose a simple yet efficient scribble-based SOD framework with a local coherence loss using color features to propagate scribble regions, and saliency structure consistency loss to predict consistent maps. However, semantic models focus on categories that pixels belong to, which could be up to tens or hundreds, while tasks like camouflage object detection (COD) only care about foreground and background objects. [6] needs to use an extra edge detector and perform training in an iterative way, and the consistency constraints used in [7] are not fully exploited, and its local coherence in camouflage data can easily mislead the model, since camouflage objects are mostly visually "unnoticeable" (*e.g.*, tiny, occluded, similar appearance with backgrounds). Therefore, these scribble-learning methods for SOD all fail to have a satisfactory prediction in COD scribble-based learning. In general, current scribble-based weakly-supervised methods are not suitable for COD.

**Weakly Supervised Salient Object Detection.** Most of the weakly supervised learning methods in salient object detection utilized two types of labels, namely image-level and point-level labels.

Methods based on image-level labels try to attain pseudo labels using techniques like CAM [13] and then build the model on it [14, 15]. Although image-level annotations are abundant and out-of-the-box, it suffers from producing accurate maps because CAM only distinguishes the most distinctive part of a class and other hand-crafted like methods cannot exploit rich information of data. On the other hand, methods with point-level labels can train models in either a similar two-stage ([16, 17]) or one-stage fashion ([18, 7, 6]). One stage approaches train the model directly from partial annotations and regularization under inductive bias. It has become popular since the appearance of gated CRF loss ([19]), which has enabled one-stage methods to perform comparably to two-stage’s, for its nature of simplicity and efficiency. For point level labels, scribble is preferred since it is nearly as easy to generate as single point annotations and produces better results.

**Camouflaged Object Detection.** COD focuses on undetectable natural objects (*e.g.*, hidden objects, tiny objects, objects with similar appearances to surroundings) and undetectable artificial objects (*e.g.*, synthetic pictures and artworks with information hiding purpose). Fan *et al.* [4] propose a COD dataset with 10K camouflaged images, which takes an average of around 60 minutes per image to annotate. Zhai *et al.* [20] design a mutual graph learning method that splits the task into rough positioning and precise boundary locating. Li *et al.* [21] apply joint learning on SOD and COD tasks, taking advantage of both tasks to meet the balance of global and local information. Mei *et al.* [22] propose a focus module to discover and remove false-positive and false-negative predictions. Yang *et al.* [5] propose a transformer-based probabilistic representational model to learn context information to solve uncertainty-guided ambiguity. However, these methods highly rely on per-pixel ground truth with full supervision, which is time-consuming and labor-intensive. To overcome these limitations, we propose structure-based scribble annotations on COD datasets, the first weakly supervised dataset for COD task to our best known. The average annotation time was reduced to about 10 seconds per image (1/360 of the fully supervised annotations).

### 3 Objective Functions for COD

Noticing scribble annotations make it more difficult to learn camouflaged objects’ boundary information, we propose a novel loss to improve predictions’ consistency. First, we design a feature-guided loss using semantic feature learnt from the model. To avoid much computation overhead and disturbance from noisy features, we filter the feature by measuring its significance to the prediction. We also improve the widely-adopted self-supervision-fashion cross-view consistency loss by considering the reliability bias (see Figure 4 (a)). Soft inside-view consistency and CRF-like ([19] image feature guided loss are also applied.

#### 3.1 Consistency Loss

Weakly supervised methods often suffer from inconsistent predictions, particularly in the field of COD to our observation. The visual similarity between background and foreground easily confuses the model. Self-supervised learning tries to alleviate such inconsistency by computing the difference between the network representation of the input and its transformation as constraint loss [23, 24]. Recently, weakly supervised methods also include similar loss [7, 12]. However, there are still limitations to the application of these losses in scribble-based weakly supervised learning: (1) The combination of transforms is not well explored. Some are using resize [7] and others are using flipping, translation [12]. (2) The reliability of the representation is ignored. To our observation, the predictions of the original input are often better than its transform, as shown in Figure 4 (a). (3) Consistency inside the single map is not considered. To overcome these, we propose two consistency constraints, namely cross-view consistency and inside-view consistency, and explore variations to optimize them. Compared with others, our method imposes stronger and more exact consistency to the model without the need for auxiliary well-annotated datasets or well-trained detectors.

**Reliable cross-view consistency loss.** A good object detection model should be able to locate the same objects in images, even after transformations are applied. To ensure the property, we define a cross-view loss for it. For a neural network function  $f_\theta(\cdot)$  with parameter  $\theta$ , some transformations  $T(\cdot)$ , input  $x$ , the ideal situation is:

$$f_\theta(T(x)) = T(f_\theta(x)) \quad (1)$$



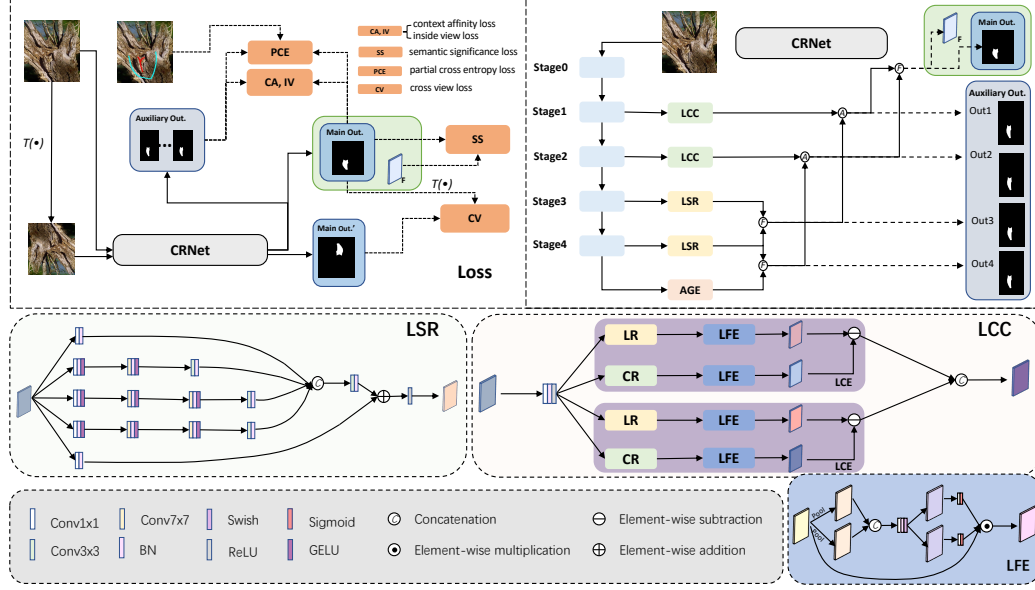


Figure 3: An overview of our proposed method. The loss composes of 5 parts, mainly focusing on reliable consistency and following guidance from semantic features learnt by the model.  $F, T(\cdot)$  are the feature map extracted before predictions and the transform function to input. Our contrast and relation network (CRNet) applies local-context contrasted modules (LCC) at the second and third stages, logical semantic relation modules (LSR) at the last two stages, and the auxiliary global extractor (AGE) at the last stage.

Taking (1) as regularization, we use the similar consistent loss inherited from [7], where SSIM is single scale SSIM ([25]),  $\alpha$  is 0.85,  $P, \hat{P}$  are prediction maps for input and its transform,  $M$  is the total number of pixels and  $i, j$  is the index of a pixel in each map.

$$L_{cv} = \frac{1}{M} \sum_{i,j} (1 - \alpha) \frac{1 - SSIM(P_{ij}, \hat{P}_{ij})}{2} + \alpha |P_{ij} - \hat{P}_{ij}| \quad (2)$$

As the above mentioned reliability bias, we specifically hope the predictions  $\hat{P}$  get close to  $P$  instead of vice versa. The key here is to weight their backward gradient differently by computing the loss with the detached predictions twice, respectively. To elaborate on this, (2) can be written as

$$L_{cv1} = \frac{1}{M} \sum_{i,j} (1 - \alpha) \frac{1 - SSIM(P_{ij}^d, \hat{P}_{ij})}{2} + \alpha |P_{ij}^d - \hat{P}_{ij}| \quad (3)$$

$$L_{cv2} = \frac{1}{M} \sum_{i,j} (1 - \alpha) \frac{1 - SSIM(P_{ij}, \hat{P}_{ij}^d)}{2} + \alpha |P_{ij} - \hat{P}_{ij}^d| \quad (4)$$

$$L_{cv} = L_{cv1} + L_{cv2} \quad (5)$$

where  $P^d, \hat{P}^d$  means the detach operation that stops the gradient on variable. If the prediction  $P$  is more reliable than  $\hat{P}$ , the gradient for  $P$  should be smaller than  $\hat{P}$ . Thus, the reliable cross-view consistency is proposed as  $L_{rcv} = (1 + \gamma)L_{cv1} + (1 - \gamma)L_{cv2}$ , when  $\gamma = 0$ ,  $L_{cv} = L_{rcv}$ .  $\gamma$  is set to 0.3 in practice.

**Soft inside-view consistency loss.** Moreover, we noticed that apart from the cross-view consistency, inside-view consistency is also important. The term inside-view means the predicting consistency inside a single prediction map. For the inside of an object, we also want consistent predictions, which is either salient or non-salient in this specific task; but in parts near the boundary, forcing the model to predict confidently is misleading. We use the entropy to force the model to predict inside-object parts confidently. Here, we use a soft indicator to filter noisy predictions: when the entropy above a

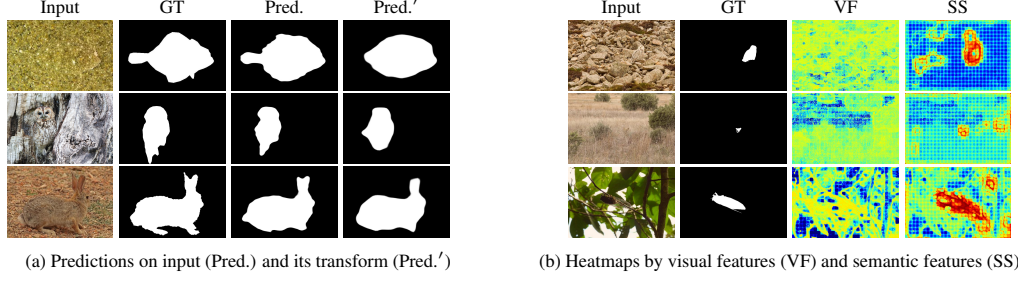


Figure 4: In the regularization of consistency, prediction on images has different reliability. (a) clearly shows that prediction on original input is much more accurate. Therefore, it improves the model performance by inducing this reliability bias in our loss design; Camouflage objects often cannot be distinguished by simple visual features (*e.g.* RGB colors and positions). In (b) we divide the pictures into  $16 \times 16$  blocks with stride 16, and accumulate different kernel values of every pixel in its blocks. The hot color indicates a significant difference with the surroundings. (b) shows that semantic features extracted are able to locate camouflaged objects.

certain threshold, we regard that pixel as a near-boundary region for its difficulty to predict. The soft inside-view consistency loss is as below.

$$L_{iv} = w_{iv} \cdot \frac{1}{|I - \mathcal{B}|} \sum_{(i,j) \in I - \mathcal{B}} -P_{ij} \log P_{ij} - (1 - P_{ij}) \log(1 - P_{ij}) \quad (6)$$

where  $I, \mathcal{B}$  are the set of all pixels and near-boundary pixels,  $w_{iv}$  is the weight of this loss and set to 0.05 in practice. The entropy threshold for the near-boundary pixel is 0.5. Notice that we add this loss in the late stage of training, when the prediction is relatively accurate.

Combined with all the consistency loss, we have the final consistency loss  $L_{cst} = L_{rcv} + L_{iv}$ .

### 3.2 Feature-guided Loss

Scribble-based methods often suffer from the lack of object information provided by limited labeled data. A large portion of images is unlabeled, leaving rich information embedded in those regions unexploited and causing non-smooth boundary. To tackle the problem, gated CRF loss ([19]) has been proposed. It exploits the information by using the image's pixel features like colors and positions. This might be useful in the context of SOD [7], where the foreground object has visually distinctive boundaries from the background. However, in camouflage object detection, similarity in such visual features is no longer a clear cue since objects are "camouflaged". Although it may still be hard to locate camouflage objects at first sight, humans can easily recognize them and their boundary with a few pixels annotated. This is because we extract higher semantic information in mind and know what features are significant according to the semantics of surroundings and objects. Therefore, we design feature guided loss based on both simple pixel features (context affinity loss) and complex features learnt by a neural network (semantic significance loss), aiming to predict clear boundaries in camouflage object detection. As shown in Figure 4 (b), the semantic we extracted from the learned models enables itself to focus on "camouflaged" boundary regions.

**Context affinity loss.** Nearby pixels with similar feature tends to have the same category. This simple idea introduces the context affinity loss. We first notice that the pixels too far away have nearly no relation at all, so we focus our loss in a  $n \times n$  region for one specific pixel. Then, we adopt the kernel method in [19] to measure the visual feature similarity (colors and positions), which is defined as:

$$K_{vis}(i, j) = \exp\left(-\frac{\|S(i) - S(j)\|^2}{2\sigma_S^2} - \frac{\|C(i) - C(j)\|^2}{2\sigma_C^2}\right) \quad (7)$$

where  $S(i), C(i)$  is the position and colors of the pixel  $i$ ,  $\sigma_S, \sigma_C$  are hyperparameters. The idea is to make similar pixels have similar predictions so context affinity loss  $L_{ca}$  can be written as:

$$D(i, j) = 1 - P_i P_j - (1 - P_i)(1 - P_j) \quad (8)$$

$$L_{ca} = \frac{1}{M} \sum_i \frac{1}{K_d(i)} \sum_{j \in K_d(i)} K_{vis}(i, j) D(i, j) \quad (9)$$

where  $K_d(i)$  is the neighbor  $n \times n$  regions centering pixel  $i$ . Through context affinity loss, the model can quickly learn from the whole image and produce relatively good predictions.

**Semantic significance loss.** As mentioned above, visual cues around boundaries might not be strong enough in camouflage object detection. We can mimic how humans recognize objects, using higher semantic information and more significant features between pixels to solve the problem. Here, the feature map  $F \in \mathbb{R}^{H \times W \times C}$  is extracted before the final prediction layer.<sup>2</sup> The significance of a feature channel is determined by its covariance with predictions.

$$Sig_i = cov(F_i, P), i \in \{1, \dots, C\} \quad (10)$$

where  $F_i$  is the feature map of the  $i$ -th channel. Then we take the top  $N$  channels ordered by  $Sig$  to form feature map  $\hat{F} \in \mathbb{R}^{H \times W \times N}$ , which represents the significant features with both semantic and low-level information. Also, the model should focus on the boundary region. A region is defined as a boundary region if it has at least 30% of the pixels classified as foreground and background (if a pixel has scribble annotation or model prediction above 0.8 then it is classified). The semantic significance loss has a similar formulation to context affinity loss.

$$K_{sem} = \exp\left(-\frac{\|S(i) - S(j)\|^2}{2\sigma_S^2} - \frac{\|\hat{F}(i) - \hat{F}(j)\|^2}{2\sigma_C^2}\right) \quad (11)$$

$$L_{ss} = w_{ss} \frac{1}{M} \sum_k \frac{1}{|R_k|} \sum_{i, j \in R_k} K_{sem}(i, j) D(i, j) \quad (12)$$

where  $R_k$  is the valid boundary regions (in practice, we divide an image to equal  $20 \times 20$  size blocks for more efficient computation and memory use),  $w_{ss}$  is a hyperparameter increasing with the epoch number since the model have not yet learnt well represented features in the beginning.

In conclusion, the feature loss  $L_{ft}$  can be written as the sum of both loss in  $L_{ft} = L_{ca} + L_{ss}$ .

### 3.3 Objective Function

As shown in Figure 3, our final objective function consists of supervisions for multiple output. For the main output out0, we combine all the above loss functions as well as the partial cross-entropy (PCE) loss to impose the strongest supervision. Below is PCE loss where  $\tilde{P}$  is the set of labeled pixels in scribble map,  $y_i$  is the true class of pixel  $i$  while  $\hat{y}_i$  is the predictions on pixel  $i$ .

$$L_{pce} = \frac{1}{N} \sum_{i \in \tilde{P}} -y_i \log \hat{y}_i - (1 - y_i) \log(1 - \hat{y}_i) \quad (13)$$

For the auxiliary outputs (from Out1 to Out4), we observe that semantic significance loss hardly improves the performance due to the inaccurate representation and cross-view consistency does not bring much benefit since it is already guaranteed in the main output. Therefore, to achieve a good balance between efficiency and accuracy, we design the auxiliary loss with only inside-view consistency and context affinity loss.  $L_{aux}^i = L_{pce}^i + L_{ca}^i + L_{iv}^i (i = 1, 2, 3, 4)$ , where  $L_x^i$  is the loss function applied to that specific auxiliary output. Note that every output is upsampled by 2d interpolation to the same size as the input. Finally, the total objective function of our output is:

$$L = L_{cst} + L_{ft} + L_{pce} + \sum_{i=1}^4 \beta_i L_{aux}^i \quad (14)$$

<sup>2</sup>For example, if the final layer is a  $3 \times 3$  convolution layer with input channel 64, output channel 1 (1 since it is binary segmentation), it can be seen as first achieving  $F$  through a  $3 \times 3$  conv layer with 64 input channels, 64 output channels in 64 groups, and then getting  $P$  by a sum pooling on each channel, i.e.  $P_i = \sum_c^n F_{i,c}$  where  $i, n$  is the pixel index and channel number.

## 4 Proposed Framework

Our method for scribble learning is based on observations that camouflaged objects generally have low-level contrasts (*e.g.*, texture, color, and intensity) or logical semantic discontinuity with the background. In our network, we use ResNet-50 [26] as a backbone to extract multi-scale features. It applies a local-context contrasted module (LCC) that enhances low-level contrasts and sharpness to expand potential camouflaged regions. We also propose a logical semantic relation module (LSR) to finalize the objects. The overall framework is shown in Figure 3. The training dataset is defined as  $D = \{x_n, y_n\}_{n=1}^N$ , where  $x_n$  is the input,  $y_n$  is the corresponding binary map, and  $N$  is the total number of training images. In our task,  $y_n$  is in scribble-form.

We first feed the input image to the backbone ResNet-50 [26] and an auxiliary global extractor (AGE) to obtain multi-scale input features  $f_i$ , where  $i \in \{x | 0 \leq x \leq 4, x \in \mathbb{N}\}$  denotes the stage of backbone. The AGE is a pyramid pooling module [27] substituting with GELU activation functions. Our method uses low-level input features  $F_1$  and  $F_2$  to extract contrasted features  $F_c^0$  and  $F_c^1$ , high-level input features  $F_3$  and  $F_4$  to learn logical semantic information  $F_s^0$  and  $F_s^1$ . In addition, we use an AGE to further acquire global semantic information  $F_s^g$ . Fusing  $F_s^1$  with  $F_s^0$  and  $F_s^g$ , we further process logical semantic information as  $F_l^0$  and  $F_l^1$ , respectively. After aggregating  $F_c^0$  with  $F_l^0$  to  $F_{out}^0$ ,  $F_c^1$  with  $F_l^1$  to  $F_{out}^1$ . The final output camouflaged map is the fusion of  $F_{out}^0$  and  $F_{out}^1$  processed by a  $3 \times 3$  convolution.

The AGE is a pyramid pooling module [27] with GELU activation functions. It contains four levels of adaptive average pooling layers with output sizes  $1 \times 1$ ,  $2 \times 2$ ,  $3 \times 3$ ,  $6 \times 6$ , respectively. We then take the pooling feature in each level into a  $1 \times 1$  convolution, reducing the channel number to  $\frac{1}{4}$ . After concatenating four-level output features with the original module input feature, we adopt a  $1 \times 1$  convolutional layer for performing the final output. All convolutional layers in AGE are followed by batch normalization and GELU function.

### 4.1 Local-Context Contrasted (LCC) Module

Camouflaged objects usually have different low-level features (*e.g.*, texture, color, intensity) with backgrounds. Visual inhibition on the mammalian retina enhances the sharpness and contrast in visual response [10]. Inspired by it, we propose a local-context contrasted module which inhibits neighbor’s activity. Here, we use two inhibited low-level contrasted extractors (LCE) on different receptive fields to increase contrast and sharpness. We adopt another two inhibited LCEs further strengthen low-level contrasts. The contrast information learned by LCC helps expand scribbles to potential camouflaged regions so that our method can better command the object’s primary structure and potential boundary.

LCC performs the input low-level feature  $F_{in}$  which contains informative texture, color, and intensity characteristics through two branches of low-level contrasted extractors with different receptive fields. We first reduce  $F_{in}$ ’s channel number to 64 by a  $1 \times 1$  convolutional layer with batch normalization and ReLU, and then take the obtained  $F_{low} \in 64 \times H \times W$  to two low-level contrasted extractors (LCE) focus on different sizes of fields. An LCE consists of a local receptor (LR), a context receptor (CR), and two low-level feature extractors (LFE). The  $F_{low}$  goes through an LR which is a  $3 \times 3$  convolutional layer with 1 dilation rate and an LFE to obtain the  $f_{local}$ . Meanwhile,  $f_{low}$  is also extracted by a CR which is a  $3 \times 3$  convolutional layer with dilation  $d_{context}$  and further by an LFE for  $f_{context}$ . We take the subtraction of  $f_{local}$  and  $f_{context}$  into batch normalization and ReLU to get one level contrasted feature  $f_{contrast}$ . We set the  $d_{context}$  to 4 and 8 for two level of LCE, extracting low-level contrasted features  $f_{contrast}^1$  and  $f_{contrast}^2$  concentrating on different sizes of receptive fields. The final output is a concatenation of  $f_{contrast}^1$  and  $f_{contrast}^2$ .

$$F_{low} = \mathcal{R}(\mathcal{N}(f_1(F_{in}, \theta_1))) \quad (15)$$

$$F_c^0 = \mathcal{R}(\mathcal{N}(LFE(f_l^0(F_{low}, \theta_l^0), \alpha_0^0) - LFE(f_c^0(F_{low}, \theta_c^0), \alpha_1^1, d_{context} = 4))) \quad (16)$$

$$F_c^1 = \mathcal{R}(\mathcal{N}(LFE(f_l^1(F_{low}, \theta_l^1), \alpha_1^0) - LFE(f_c^1(F_{low}, \theta_c^1), \alpha_1^1, d_{context} = 8))) \quad (17)$$

$$F_c^{out} = F_c^0 \odot F_c^1 \quad (18)$$

Inspired by the cross-channel direction and position sensitive strategy proposed by Hou *et al.* [28], we adopt a crossing spatial and channel attention mechanism in LFE to extract low-level features

(e.g., texture, intensity, color). The input feature  $F_{in}$  is firstly taken into a 1-dimensional horizontal and vertical global pooling separately. We use a  $1 \times 1$  convolutional layer, batch normalization and Swish function to process the concatenation of two pooling results. Then the processed feature  $F_{mid}$  is split to  $F_{mid}^h \in C \times H \times 1$  and  $F_{mid}^w \in C \times 1 \times W$  with permutation.  $F_{mid}^h$  and  $F_{mid}^w$  go through a  $1 \times 1$  convolutional layer and Sigmoid, before multiplying together with  $F_{in}$  as an output.

$$F_{mid} = Swish(\mathcal{N}(f_1(\mathcal{P}_h(F_{in}) \odot \text{permute}(\mathcal{P}_w(F_{in})), \theta_1))) \quad (19)$$

$$F_{mid}^h, F_{mid}^w = \text{split}(F_{mid}) \quad (20)$$

$$F_{out} = F_{in} \odot Sigmoid(f_h(F_{mid}^h, \theta_h)) \odot Sigmoid(f_w(\text{permute}(F_{mid}^w), \theta_w)) \quad (21)$$

## 4.2 Logical Semantic Relation (LSR) Module

Scribble annotation may only annotate a part of the background. When the background consists of many low-level contrasted parts (e.g., green leaves and brown branches, yellow petals, and green stems), we need logical semantic relation information to identify the real foreground and background. Hence, we propose a logical semantic relation module (LSR) to simulate the information processing, integration and abstraction (e.g., logical semantic relation) on the visual cortex [9] after accepting electronic signals (e.g., low-level contrast) [8].

LSR learns logical semantic information in 4 branches. The first branch is a single  $1 \times 1$  convolutional layer. The second branch includes the sequence of a  $1 \times 1$  convolutional layer, a  $7 \times 7$  convolutional layer with 3 paddings, and a  $3 \times 3$  convolutional layer with 7 padding, 7 dilation rate. The last two branches consist of a  $1 \times 1$  convolutional layer, two  $7 \times 7$  convolutional layers with 3 paddings, and a  $3 \times 3$  convolutional layer with 7 padding, 7 dilation rate. To be clarified, all convolutional layers are followed by a batch normalization. In addition, a GeLU is used after all convolutional layers, except for the last layers in each branch. We then use a  $3 \times 3$  convolutional layer for concatenated outputs of four branches, and add it to the input feature after a  $1 \times 1$  convolution. The final output is processed further by a GeLU function.

$$F_b^0 = \mathcal{N}(f_0^0(F_{in}, \theta_0^0)) \quad (22)$$

$$F_b^1 = \mathcal{N}(f_1^2(\mathcal{G}(\mathcal{N}(f_1^1(\mathcal{G}(\mathcal{N}(f_1^0(F_{in}, \theta_1^0))), \theta_1^1))), \theta_1^2)) \quad (23)$$

$$F_b^2 = \mathcal{N}(f_2^3(\mathcal{G}(\mathcal{N}(f_2^2(\mathcal{G}(\mathcal{N}(f_2^1(\mathcal{G}(\mathcal{N}(f_2^0(F_{in}, \theta_2^0))), \theta_2^1))), \theta_2^2))), \theta_2^3)) \quad (24)$$

$$F_b^3 = \mathcal{N}(f_3^3(\mathcal{G}(\mathcal{N}(f_3^2(\mathcal{G}(\mathcal{N}(f_3^1(\mathcal{G}(\mathcal{N}(f_3^0(F_{in}, \theta_3^0))), \theta_3^1))), \theta_3^2))), \theta_3^3)) \quad (25)$$

$$F_{logic}^{mid} = \mathcal{N}(f_c(F_b^0 \odot F_b^1 \odot F_b^2 \odot F_b^3, \theta_c)) \quad (26)$$

$$F_{logic}^{out} = \mathcal{R}(F_{logic}^{mid} \oplus f_{res}(F_{in}, \theta_{res})) \quad (27)$$

## 5 Experiments

**Implementation Details.** Our experiments are conducted on three COD benchmarks, CAMO[29], CHAMELEON[30], and COD10K[4]. Following previous studies [4, 22, 20], we use 4,040 images (3,040 from COD10K, 1,000 from CAMO) for training, and the remaining for testing. We adopt four evaluation metrics: Mean Absolute Error (MAE), S-measure  $S_m$  [31], E-measure ( $E_m$ ) [32] and weighted F-measure  $F_\beta^w$  [33]. We implement our method with PyTorch and conduct experiments on a GeForce RTX2080Ti GPU. Input images are resized to  $320 \times 320$  with horizontal flips during the training process. We use the stochastic gradient descent (SGD) optimizer with a momentum value of 0.9 and a weight decay of  $5e-4$ . In the training phase, we use triangle learning rate scheduling and the maximum learning rate is  $1e-3$ , the batch size is 16, and the training epoch is 150. It takes around 5 hours to train. As for the inference process, input images are only resized to  $320 \times 320$  and then directly predict final maps without any post-processing (e.g., CRF).

**Comparison with State-of-the-arts.** As we propose the first weakly supervised method, we introduce 2 scribble-based weakly and 2 unsupervised salient object detection for comparison. We also provide the results of fully supervised 7 COD and 12 SOD methods as a reference. Quantitative comparisons are demonstrated in Table 1. Our method performs best under four metrics on

Table 1: Quantitative comparisons with state-of-the-arts on three benchmarks. “F”, “U”, and “W” denote fully-supervised, unsupervised, and weakly-supervised, respectively.

Methods	Sup.	CAMO[29]				CHAMELEON[30]				COD10K[4]			
		MAE↓	$S_m$ ↑	$E_m$ ↑	$F_\beta^w$ ↑	MAE↓	$S_m$ ↑	$E_m$ ↑	$F_\beta^w$ ↑	MAE↓	$S_m$ ↑	$E_m$ ↑	$F_\beta^w$ ↑
NLDF[34]	F	0.123	0.665	0.664	0.495	0.063	0.798	0.809	0.652	0.059	0.701	0.709	0.473
PiCANet[35]	F	0.125	0.701	0.716	0.510	0.085	0.765	0.778	0.552	0.081	0.696	0.712	0.415
CPD[36]	F	0.113	0.716	0.723	0.556	0.048	0.857	0.874	0.731	0.053	0.750	0.776	0.531
EGNet[37]	F	0.109	0.732	0.800	0.604	0.065	0.797	0.860	0.649	0.061	0.736	0.810	0.517
PoolNet[38]	F	0.105	0.730	0.746	0.575	0.054	0.845	0.863	0.690	0.056	0.740	0.776	0.506
SCRN[41]	F	0.090	0.779	0.797	0.643	0.042	0.876	0.889	0.741	0.047	0.789	0.817	0.575
F3Net[39]	F	0.109	0.711	0.741	0.564	0.047	0.848	0.894	0.744	0.051	0.739	0.795	0.544
CSNet[42]	F	0.092	0.771	0.795	0.641	0.047	0.856	0.868	0.718	0.047	0.778	0.809	0.569
ITSD[40]	F	0.102	0.750	0.779	0.610	0.057	0.814	0.844	0.662	0.051	0.767	0.808	0.557
MINet[43]	F	0.090	0.748	0.791	0.637	0.036	0.855	0.914	0.771	0.042	0.770	0.832	0.608
PraNet[2]	F	0.094	0.769	0.825	0.663	0.044	0.860	0.907	0.763	0.045	0.789	0.861	0.629
UCNet[44]	F	0.094	0.739	0.787	0.640	0.036	0.880	0.930	0.817	0.042	0.776	0.857	0.633
SINet[4]	F	0.092	0.745	0.804	0.644	0.034	0.872	0.936	0.806	0.043	0.776	0.864	0.631
SLSR[45]	F	0.080	0.787	0.838	0.696	0.030	0.890	0.935	0.822	0.037	0.804	0.880	0.673
MGL-R[20]	F	0.088	0.775	0.812	0.673	0.031	0.893	0.917	0.812	0.035	0.814	0.851	0.666
PFNet[22]	F	0.085	0.782	0.841	0.695	0.033	0.882	0.931	0.810	0.040	0.800	0.877	0.660
UJSC[21]	F	0.073	0.800	0.859	0.728	0.030	0.891	0.945	0.833	0.035	0.809	0.884	0.684
C2FNet[46]	F	0.080	0.796	0.854	0.719	0.032	0.888	0.935	0.828	0.036	0.813	0.890	0.686
UGTR[5]	F	0.086	0.784	0.822	0.684	0.031	0.888	0.910	0.794	0.036	0.817	0.852	0.666
USPS[47]	U	0.207	0.568	0.641	0.399	0.188	0.573	0.631	0.380	0.196	0.519	0.536	0.265
DUSD[48]	U	0.166	0.551	0.594	0.308	0.129	0.578	0.634	0.316	0.107	0.580	0.646	0.276
SS[6]	W	0.118	0.696	0.786	0.562	0.067	0.782	0.860	0.654	0.071	0.684	0.770	0.461
SCWSSOD[7]	W	0.102	0.713	0.795	0.618	0.053	0.792	0.881	0.714	0.055	0.710	0.805	0.546
Ours	W	<b>0.092</b>	<b>0.735</b>	<b>0.815</b>	<b>0.641</b>	<b>0.046</b>	<b>0.818</b>	<b>0.897</b>	<b>0.744</b>	<b>0.049</b>	<b>0.733</b>	<b>0.832</b>	<b>0.576</b>

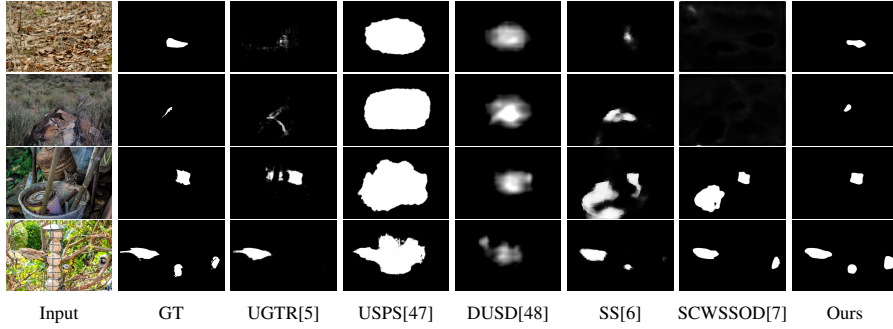


Figure 5: Qualitative comparison of our method with state-of-the-arts fully supervised, unsupervised, and scribble-based weakly supervised methods in challenging scenarios.

three benchmarks among weakly or unsupervised methods. It achieves an average enhancement of 11.0% on MAE, 3.2% on S-measure, 2.5% on E-measure, and 4.4% on weighted F-measure than the state-of-the-art method SCWSSOD [7]. Moreover, it outperforms 7 fully supervised methods [34, 35, 36, 37, 38, 39, 40]. We also find that our method has the largest improvement in CAMO (outperforms nearly all fully-supervised SOD methods and close to COD methods), which is the most challenging one among all of the 3 COD datasets (worst metric value). This shows that our method is indeed better at discovering hard camouflage objects than others. Figure 5 shows that our method performs well in various challenging scenarios, including high intrinsic similarities (row 1), tiny objects (row 2), complex backgrounds (row 3), and multiple objects (row 4).

**Ablation Studies on Loss Functions.** Detailed ablation study for loss functions is also conducted in Table 2. We first explore various combinations of transformation operations in cross-view consistency, which has not been done by previous work. We always use resizing here to reduce memory use. It is shown that with flipping, translating, and cropping upgrades the performance significantly. The third group, which is the ablation for reliability bias used in cross-view and inside-view consistency, shows improvements in all metrics except MAE and indicates the benefit of the consistency mechanism. The final group is the component ablation of consistency loss and feature-guided loss. We see that both losses provide tremendous improvement in three test datasets.

**Ablation Studies on Modules.** To verify the effectiveness of our modules, we conduct ablation studies on challenging dataset CAMO[29], where the methods obtain the worst scores according to

Table 2: The ablation study results of our loss functions. Groups correspond to ablations on transformations in cross-view consistency, on consistency loss, on feature loss, on all losses. Here, pce stands for partial cross entropy; ft, cs stands for feature-guided loss and consistency loss (cs=cv+iv, ft=ca+ss); cv, iv stands for cross-view and inside-view consistency loss and cv' means cross-view consistency without reliability bias; R,F,T,C are resizing, flipping.

Basic setting	Loss	CAMO[29]				CHAMELEON[30]				COD10K[4]			
		MAE↓	$S_m$ ↑	$E_m$ ↑	$F_{\beta}^w$ ↑	MAE↓	$S_m$ ↑	$E_m$ ↑	$F_{\beta}^w$ ↑	MAE↓	$S_m$ ↑	$E_m$ ↑	$F_{\beta}^w$ ↑
w/ pce	Baseline	0.215	0.612	0.633	0.387	0.171	0.652	0.676	0.413	0.224	0.525	0.536	0.227
w/ ft, iv	w/o cv	0.105	0.721	0.786	0.600	0.060	0.789	0.882	0.682	0.058	0.709	0.805	0.518
	w/ cv(R)	0.097	0.727	0.807	0.629	0.049	0.808	0.905	0.727	0.051	0.723	0.825	0.562
	w/ cv(R, F)	0.094	0.730	0.812	0.638	0.047	0.808	0.887	0.730	0.050	0.727	0.818	0.571
	w/ cv(R, F, T)	0.094	0.730	0.808	0.637	0.047	0.806	0.885	0.736	0.048	0.727	0.816	0.572
	w/ cv(R, F, T, C)	0.092	0.735	0.815	0.641	0.046	0.818	0.897	0.744	0.049	0.733	0.832	0.576
w/ ft	w/ cv'	0.095	0.723	0.801	0.624	0.045	0.808	0.896	0.734	0.049	0.72	0.815	0.561
	w/ cv, iv	0.095	0.726	0.804	0.632	0.043	0.814	0.907	0.740	0.048	0.729	0.821	0.574
	w/ cv, iv	0.092	0.735	0.815	0.641	0.046	0.818	0.897	0.744	0.049	0.733	0.832	0.576
w/ cs	w/ ca	0.095	0.727	0.807	0.631	0.045	0.815	0.900	0.737	0.051	0.729	0.820	0.573
	w/ ca, ss	0.092	0.735	0.815	0.641	0.046	0.818	0.897	0.744	0.049	0.733	0.832	0.576
w/ pce	w/ cs	0.096	0.731	0.821	0.641	0.050	0.805	0.899	0.723	0.051	0.726	0.835	0.567
	w/ ft	0.107	0.720	0.785	0.592	0.063	0.794	0.872	0.674	0.058	0.713	0.803	0.519
	w/ cs, ft	0.092	0.735	0.815	0.641	0.046	0.818	0.897	0.744	0.049	0.733	0.832	0.576

Table 3: The ablation study results of components on CAMO[29].

Methods	BB	AGE	LCC	LSR	MAE↓	$S_m$ ↑	$E_m$ ↑	$F_{\beta}^w$ ↑
Ablation I	✓				0.104	0.701	0.774	0.598
Ablation II	✓	✓			0.100	0.716	0.799	0.615
Ablation III	✓	✓	✓		0.099	0.721	0.806	0.626
Ablation IV	✓	✓		✓	0.098	0.713	0.783	0.612
Ours	✓	✓	✓	✓	0.092	0.735	0.815	0.641

Table 1. Table 3 shows only using a backbone (BB) performs worst (*i.e.*, Ablation I), while adding LCC or LSR improves performances on different metrics. As an example shown in Figure 6, LCC finds potential camouflaged regions with low-level contrasts, but it may be confused by complex background (*e.g.*, many distinct leaves). Meanwhile, LSR analyzes logical semantic relations between different parts, but it may segment inaccurate boundaries. Our method achieves the best performance with all proposed modules.



Figure 6: A visual example of the component ablation study.

## 6 Conclusions

In this paper, we propose the first weakly supervised COD dataset with scribble annotation which costs ~10 seconds per image (360 times faster than pixel-wise annotation). To overcome the weaknesses of current weakly supervised learning and their application to COD, we propose a novel framework consisting of two loss functions and a novel network: a consistency loss, including consistency inside and cross images, regulate the model to have coherent predictions and incline them to more reliable ones; a feature-guided loss locates the "hidden" foreground by comparing both manually computed visual features and learnt semantic features of each pixel. The proposed network learns low-level contrast to expand scribbles to wider potential regions first and then analyzes logical semantic relation information to determine the real foreground and background. Experimental results show our method outperforms unsupervised and weakly-supervised state-of-the-arts with improvement and is even competitive with the fully-supervised methods.

Our method is effective, but it has limitations. Due to scribble annotations in objects' main bodies, it performs under expectations in scenarios with intricate details in boundaries (*e.g.*, tiny intensive occlusions, slender tentacles). Figure 7 shows two examples of our failures. The first row is a cat





Figure 7: Two examples of our method’s failures that inaccurately predict complex boundaries.

occluded by tiny intensive grasses. Although our method successfully predicts the cat’s primary structure, it does not segment grasses. The second row is an animal with slender tentacles. Although our method predicts its main body and partial tentacles, which are closed to the body, it cannot detect entire tentacles. In the future, we will pay more attention to local details, especially intricate boundaries, to segment more precise camouflaged objects under weakly supervised learning.

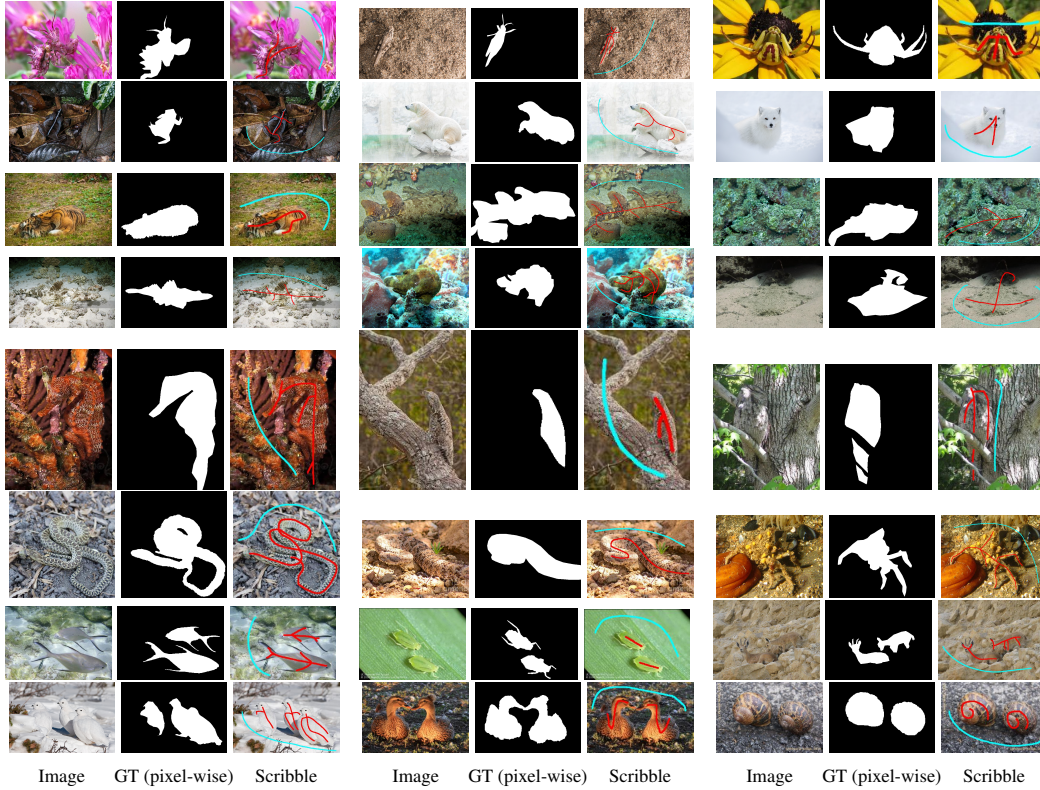


Figure 8: Examples of S-COD dataset. It includes many categories of animals in challenging scenarios.

## A S-COD Dataset

The pixel-wise annotation is time-consuming and labor-intensive. Also, it assigns equal significance to every pixel. To overcome these limitations, we propose a new dataset S-COD with scribble annotations that describe objects’ primary structures. S-COD includes 4,040 images about diverse objects (*e.g.*, Chondrichthyes, Amphibia, Reptilia, Aves, and Mammalia) in challenging scenarios (*e.g.*, similar appearance, partial occlusions, and multiple objects). See Figure 8 for examples in our dataset.



## References

- [1] Deng-Ping Fan, Tao Zhou, Ge-Peng Ji, Yi Zhou, Geng Chen, Huazhu Fu, Jianbing Shen, and Ling Shao. Inf-net: Automatic covid-19 lung infection segmentation from ct images. *IEEE Transactions on Medical Imaging*, 39(8):2626–2637, 2020.
- [2] Deng-Ping Fan, Ge-Peng Ji, Tao Zhou, Geng Chen, Huazhu Fu, Jianbing Shen, and Ling Shao. Pranet: Parallel reverse attention network for polyp segmentation. In *International conference on medical image computing and computer-assisted intervention*, pages 263–273. Springer, 2020.
- [3] Deng-Ping Fan, Ge-Peng Ji, Ming-Ming Cheng, and Ling Shao. Concealed object detection. *IEEE Transactions on Pattern Analysis and Machine Intelligence*, 2021.
- [4] Deng-Ping Fan, Ge-Peng Ji, Guolei Sun, Ming-Ming Cheng, Jianbing Shen, and Ling Shao. Camouflaged object detection. In *Proceedings of the IEEE/CVF conference on computer vision and pattern recognition*, pages 2777–2787, 2020.
- [5] Fan Yang, Qiang Zhai, Xin Li, Rui Huang, Ao Luo, Hong Cheng, and Deng-Ping Fan. Uncertainty-guided transformer reasoning for camouflaged object detection. In *Proceedings of the IEEE/CVF International Conference on Computer Vision*, pages 4146–4155, 2021.
- [6] Jing Zhang, Xin Yu, Aixuan Li, Peipei Song, Bowen Liu, and Yuchao Dai. Weakly-supervised salient object detection via scribble annotations. In *Proceedings of the IEEE/CVF conference on computer vision and pattern recognition*, pages 12546–12555, 2020.
- [7] Siyue Yu, Bingfeng Zhang, Jimin Xiao, and Eng Gee Lim. Structure-consistent weakly supervised salient object detection with local saliency coherence. In *Proceedings of the AAAI Conference on Artificial Intelligence (AAAI)*. AAAI Palo Alto, CA, USA, 2021.
- [8] George Wald. Carotenoids and the visual cycle. *The Journal of general physiology*, 19(2):351–371, 1935.
- [9] David H Hubel and Torsten N Wiesel. Receptive fields, binocular interaction and functional architecture in the cat’s visual cortex. *The Journal of physiology*, 160(1):106, 1962.
- [10] Georg Von Békésy. Sensory inhibition. In *Sensory Inhibition*. Princeton University Press, 2017.
- [11] Seungho Lee, Minhyun Lee, Jongwuk Lee, and Hyunjung Shim. Railroad is not a train: Saliency as pseudo-pixel supervision for weakly supervised semantic segmentation. In *Proceedings of the IEEE/CVF Conference on Computer Vision and Pattern Recognition*, pages 5495–5505, 2021.
- [12] Zhiyi Pan, Peng Jiang, Yunhai Wang, Changhe Tu, and Anthony G Cohn. Scribble-supervised semantic segmentation by uncertainty reduction on neural representation and self-supervision on neural eigenspace. In *Proceedings of the IEEE/CVF International Conference on Computer Vision*, pages 7416–7425, 2021.
- [13] Bolei Zhou, Aditya Khosla, Agata Lapedriza, Aude Oliva, and Antonio Torralba. Learning deep features for discriminative localization. In *Proceedings of the IEEE conference on computer vision and pattern recognition*, pages 2921–2929, 2016.
- [14] Guanbin Li, Yuan Xie, and Liang Lin. Weakly supervised salient object detection using image labels. In *Proceedings of the AAAI conference on artificial intelligence*, volume 32, 2018.
- [15] Yu Zeng, Yunzhi Zhuge, Huchuan Lu, Lihe Zhang, Mingyang Qian, and Yizhou Yu. Multi-source weak supervision for saliency detection. In *Proceedings of the IEEE/CVF conference on computer vision and pattern recognition*, pages 6074–6083, 2019.
- [16] Paul Vernaza and Manmohan Chandraker. Learning random-walk label propagation for weakly-supervised semantic segmentation. In *Proceedings of the IEEE conference on computer vision and pattern recognition*, pages 7158–7166, 2017.
- [17] Yongri Piao, Wei Wu, Miao Zhang, Yongyao Jiang, and Huchuan Lu. Noise-sensitive adversarial learning for weakly supervised salient object detection. *IEEE Transactions on Multimedia*, 2022.
- [18] Shuyong Gao, Wei Zhang, Yan Wang, Qianyu Guo, Chenglong Zhang, Yangji He, and Wenqiang Zhang. Weakly-supervised salient object detection using point supervision. *arXiv preprint arXiv:2203.11652*, 2022.

- [19] Anton Obukhov, Stamatios Georgoulis, Dengxin Dai, and Luc Van Gool. Gated crf loss for weakly supervised semantic image segmentation. *arXiv preprint arXiv:1906.04651*, 2019.
- [20] Qiang Zhai, Xin Li, Fan Yang, Chenglizhao Chen, Hong Cheng, and Deng-Ping Fan. Mutual graph learning for camouflaged object detection. In *Proceedings of the IEEE/CVF Conference on Computer Vision and Pattern Recognition*, pages 12997–13007, 2021.
- [21] Aixuan Li, Jing Zhang, Yunqiu Lv, Bowen Liu, Tong Zhang, and Yuchao Dai. Uncertainty-aware joint salient object and camouflaged object detection. In *Proceedings of the IEEE/CVF Conference on Computer Vision and Pattern Recognition*, pages 10071–10081, 2021.
- [22] Haiyang Mei, Ge-Peng Ji, Ziqi Wei, Xin Yang, Xiaopeng Wei, and Deng-Ping Fan. Camouflaged object segmentation with distraction mining. In *Proceedings of the IEEE/CVF Conference on Computer Vision and Pattern Recognition*, pages 8772–8781, 2021.
- [23] Samuli Laine and Timo Aila. Temporal ensembling for semi-supervised learning. *arXiv preprint arXiv:1610.02242*, 2016.
- [24] Sudhanshu Mittal, Maxim Tatarchenko, and Thomas Brox. Semi-supervised semantic segmentation with high-and low-level consistency. *IEEE transactions on pattern analysis and machine intelligence*, 43(4):1369–1379, 2019.
- [25] Clément Godard, Oisin Mac Aodha, and Gabriel J Brostow. Unsupervised monocular depth estimation with left-right consistency. In *Proceedings of the IEEE conference on computer vision and pattern recognition*, pages 270–279, 2017.
- [26] Kaiming He, Xiangyu Zhang, Shaoqing Ren, and Jian Sun. Deep residual learning for image recognition. In *Proceedings of the IEEE conference on computer vision and pattern recognition*, pages 770–778, 2016.
- [27] Hengshuang Zhao, Jianping Shi, Xiaojuan Qi, Xiaogang Wang, and Jiaya Jia. Pyramid scene parsing network. In *Proceedings of the IEEE conference on computer vision and pattern recognition*, pages 2881–2890, 2017.
- [28] Qibin Hou, Daquan Zhou, and Jiashi Feng. Coordinate attention for efficient mobile network design. In *Proceedings of the IEEE/CVF Conference on Computer Vision and Pattern Recognition*, pages 13713–13722, 2021.
- [29] Trung-Nghia Le, Tam V Nguyen, Zhongliang Nie, Minh-Triet Tran, and Akihiro Sugimoto. Anabran network for camouflaged object segmentation. *Computer Vision and Image Understanding*, 184:45–56, 2019.
- [30] Przemysław Skurowski, Hassan Abdulameer, J Błaszczyk, Tomasz Depta, Adam Kornacki, and P Koziel. Animal camouflage analysis: Chameleon database. *Unpublished manuscript*, 2(6):7, 2018.
- [31] Deng-Ping Fan, Ming-Ming Cheng, Yun Liu, Tao Li, and Ali Borji. Structure-measure: A new way to evaluate foreground maps. In *Proceedings of the IEEE international conference on computer vision*, pages 4548–4557, 2017.
- [32] Deng-Ping Fan, Cheng Gong, Yang Cao, Bo Ren, Ming-Ming Cheng, and Ali Borji. Enhanced-alignment measure for binary foreground map evaluation. *arXiv preprint arXiv:1805.10421*, 2018.
- [33] Ran Margolin, Lihi Zelnik-Manor, and Ayellet Tal. How to evaluate foreground maps? In *Proceedings of the IEEE conference on computer vision and pattern recognition*, pages 248–255, 2014.
- [34] Zhiming Luo, Akshaya Mishra, Andrew Achkar, Justin Eichel, Shaozi Li, and Pierre-Marc Jodoin. Non-local deep features for salient object detection. In *Proceedings of the IEEE Conference on computer vision and pattern recognition*, pages 6609–6617, 2017.
- [35] Nian Liu, Junwei Han, and Ming-Hsuan Yang. Picanet: Learning pixel-wise contextual attention for saliency detection. In *Proceedings of the IEEE conference on computer vision and pattern recognition*, pages 3089–3098, 2018.
- [36] Zhe Wu, Li Su, and Qingming Huang. Cascaded partial decoder for fast and accurate salient object detection. In *Proceedings of the IEEE/CVF conference on computer vision and pattern recognition*, pages 3907–3916, 2019.

- [37] Jia-Xing Zhao, Jiang-Jiang Liu, Deng-Ping Fan, Yang Cao, Jufeng Yang, and Ming-Ming Cheng. Egnet: Edge guidance network for salient object detection. In *Proceedings of the IEEE/CVF international conference on computer vision*, pages 8779–8788, 2019.
- [38] Jiang-Jiang Liu, Qibin Hou, Ming-Ming Cheng, Jiashi Feng, and Jianmin Jiang. A simple pooling-based design for real-time salient object detection. In *Proceedings of the IEEE/CVF conference on computer vision and pattern recognition*, pages 3917–3926, 2019.
- [39] Jun Wei, Shuhui Wang, and Qingming Huang. F<sup>3</sup>net: fusion, feedback and focus for salient object detection. In *Proceedings of the AAAI Conference on Artificial Intelligence*, volume 34, pages 12321–12328, 2020.
- [40] Huajun Zhou, Xiaohua Xie, Jian-Huang Lai, Zixuan Chen, and Lingxiao Yang. Interactive two-stream decoder for accurate and fast saliency detection. In *Proceedings of the IEEE/CVF Conference on Computer Vision and Pattern Recognition*, pages 9141–9150, 2020.
- [41] Zhe Wu, Li Su, and Qingming Huang. Stacked cross refinement network for edge-aware salient object detection. In *Proceedings of the IEEE/CVF international conference on computer vision*, pages 7264–7273, 2019.
- [42] Shang-Hua Gao, Yong-Qiang Tan, Ming-Ming Cheng, Chengze Lu, Yunpeng Chen, and Shuicheng Yan. Highly efficient salient object detection with 100k parameters. In *European Conference on Computer Vision*, pages 702–721. Springer, 2020.
- [43] Youwei Pang, Xiaoqi Zhao, Lihe Zhang, and Huchuan Lu. Multi-scale interactive network for salient object detection. In *Proceedings of the IEEE/CVF conference on computer vision and pattern recognition*, pages 9413–9422, 2020.
- [44] Jing Zhang, Deng-Ping Fan, Yuchao Dai, Saeed Anwar, Fatemeh Sadat Saleh, Tong Zhang, and Nick Barnes. Uc-net: Uncertainty inspired rgb-d saliency detection via conditional variational autoencoders. In *Proceedings of the IEEE/CVF conference on computer vision and pattern recognition*, pages 8582–8591, 2020.
- [45] Yunqiu Lv, Jing Zhang, Yuchao Dai, Aixuan Li, Bowen Liu, Nick Barnes, and Deng-Ping Fan. Simultaneously localize, segment and rank the camouflaged objects. In *Proceedings of the IEEE/CVF Conference on Computer Vision and Pattern Recognition*, pages 11591–11601, 2021.
- [46] Yujia Sun, Geng Chen, Tao Zhou, Yi Zhang, and Nian Liu. Context-aware cross-level fusion network for camouflaged object detection. *arXiv preprint arXiv:2105.12555*, 2021.
- [47] Tam Nguyen, Maximilian Dax, Chaithanya Kumar Mummadi, Nhung Ngo, Thi Hoai Phuong Nguyen, Zhongyu Lou, and Thomas Brox. Deepusps: Deep robust unsupervised saliency prediction via self-supervision. *Advances in Neural Information Processing Systems*, 32, 2019.
- [48] Jing Zhang, Tong Zhang, Yuchao Dai, Mehrtash Harandi, and Richard Hartley. Deep unsupervised saliency detection: A multiple noisy labeling perspective. In *Proceedings of the IEEE conference on computer vision and pattern recognition*, pages 9029–9038, 2018.